Applied Physics Letters

RESEARCH ARTICLE | AUGUST 18 2022

Enhanced growth and properties of non-catalytic GaAs nanowires via Sb surfactant effects

A. Ajay ; H. Jeong ; T. Schreitmüller ; M. Döblinger; D. Ruhstorfer; N. Mukhundhan; P. A. L. M. Koolen; J. J. Finley ; G. Koblmüller

Appl. Phys. Lett. 121, 072107 (2022)
https://doi.org/10.1063/5.0095952

AIP Publishing

Applied Physics Letters ARTICLE scitation.org/journal/apl

Enhanced growth and properties of non-catalytic GaAs nanowires via Sb surfactant effects

Cite as: Appl. Phys. Lett. **121**, 072107 (2022); doi: 10.1063/5.0095952
Submitted: 14 April 2022 · Accepted: 30 July 2022 ·
Published Online: 18 August 2022

A. Ajay,[1,a] H. Jeong,[1] T. Schreitmüller,[1] M. Döblinger,[2] D. Ruhstorfer,[1] N. Mukhundhan,[1] P. A. L. M. Koolen,[1] J. J. Finley,[1] and G. Koblmüller[1,a]

AFFILIATIONS

[1]Walter Schottky Institute and Physics Department, Technical University of Munich, Garching, Germany
[2]Department of Chemistry, Ludwig-Maximilians-University Munich, Munich, Germany

[a]Authors to whom correspondence should be addressed: Akhil.Ajay@wsi.tum.de and Gregor.Koblmueller@wsi.tum.de

ABSTRACT

We report the effects of antimony (Sb) surfactant on the growth and correlated structural and optical properties of non-catalytic GaAs nanowires (NW) grown by selective area epitaxy on silicon. Strong enhancements in the axial growth with very high aspect ratio up to 50 are observed by the addition of small traces of Sb (1%–2%), contrasting the commonly reported growth limiting behavior of Sb in GaAs(Sb) NWs. The Sb surfactant effect modifies the growth facet structure from a pyramidal-shaped growth front terminated by {1–1–0} planes to a flat (111)B growth plane, that is even further improved by the presence of Si co-dopants. Additional benefits are seen by the substantial change in microstructure, from a heavily defected layer stacking in Sb-free GaAs NWs to a twinned phase-pure zinc blende structure in Sb-mediated GaAs(Sb) NWs. We directly confirm the impact of the altered microstructure on the optical emission and carrier recombination dynamics via observation of long, few-ns carrier lifetimes in the GaAs(Sb) NWs using steady-state and time-resolved photoluminescence spectroscopy.

GaAs-based nanowires (NW) have evolved as prosperous materials for advanced Si-integrated device applications, evidenced by recent development of ultrafast on-chip nano-lasers,[1–3] deterministic quantum light sources,[4–6] third-generation solar cells and high-speed photodetectors,[7–9] as well as high-mobility transistors on Si.[10,11] Much of this progress is owed to the availability of different fabrication/growth methods, where key challenges lie in the realization of scalable NW arrays with high uniformity, structural integrity and excellent control of aspect ratio, doping, and heterostructure formation.

Both vapor–liquid–solid (VLS) and droplet-free vapor–solid (VS) growth processes were explored, each of these facing different challenges. VLS-type growth of GaAs NWs is especially hampered by limitations in creating abrupt heterointerfaces and doping profiles along the growth axis,[12–14] and coping with large sensitivities of the NW morphology (tapering) and crystal/defect structure on kinetically dynamic variations of droplet size and contact angle during growth.[15–18] These factors pose large implications on the homogeneity of electronic and optical properties,[19,20] as ready transitions in the crystal phase (zinc blende—ZB and wurtzite—WZ) and the formation of multiphase NWs are observed.

Pure vapor–solid growth can circumvent these issues, as demonstrated by early studies of selective area MOVPE (metal-organic vapor phase epitaxy) growth.[21,22] Such non-catalytic, selective area epitaxy (SAE) was recently also realized for molecular beam epitaxial (MBE) growth on SiO_2-masked Si using extremely high V/III ratios.[23] Hereby, growth proceeds spontaneously without any tapering and with rates governed by the available group-III supply.[24] Another advantage is that doping of VS-type GaAs NWs typically yields the desired electrical activity: for example, doping by silicon (Si) leads to expected n-type behavior,[21,23] unlike for VLS-type growth.[25,26] Despite these promises, VS-type GaAs NWs suffer, however, from kinetic limitations resulting in large radial growth and poor aspect ratios (NW length/diameter) of only ∼5–10, even for extended growth times.[23,24] Also, they exhibit heavy stacking disorder of mixed cubic and hexagonal phase components, which induce detrimental multiple emission peak signatures in photoluminescence (PL) spectra.[23]

Introducing surfactants is an intriguing way to modify growth dynamics and resulting structural and electronic properties, as shown for the planar growth of GaAs and active GaInAs/GaAs heterostructures.[27,28] For GaAs NWs, surfactant-mediated growth was only

conducted for VLS-type NWs, especially by the use of antimony (Sb) surfactant. Here, the presence of Sb yields predominantly ZB crystal phase, but at the expense of substantially increased radial growth.[29,30] Such enhanced lateral growth along the {1–10} sidewall facets coincides with previous observations of patterned GaAs growth in the presence of Sb.[28] Interestingly, there are no studies yet on the effect of Sb on the growth of non-VLS GaAs NWs.

In this Letter, we report a hitherto unexpected Sb self-surfactant effect that drastically enhances axial growth, resulting in very high aspect ratios of >50 and specular end facets in periodic arrays of non-VLS GaAs(Sb) NWs. To elaborate these unique findings, we systematically analyze morphology and microstructure evolution by small additions of Sb to the growth of GaAs NWs—also under the influence of Si doping and in dependence of the SAE-based pattern geometry. Hereby, we highlight important improvements of the microstructure under the presence of Sb that establishes pure ZB-phase domains, and further study its impact on the optical properties using steady-state and time-resolved PL spectroscopy.

All NW growth was carried out in a solid-source Gen-II MBE system equipped with conventional effusion cells for group-III elements (In, Ga, Al) and Veeco valved cracker cells for supply of group-V elements arsenic (As) and antimony (Sb). The supply of As species was provided by uncracked As_4, and the Sb species were supplied as Sb_2 molecules. For the SAE-type growth, single-side polished 2-in. p-type Si (111) wafers were used with a 20-nm-thick thermally grown SiO_2 mask layer on top. Each substrate was prepatterned identically using electron beam lithography (EBL) and reactive ion etching (RIE) to produce periodic mask patterns arranged in hexagonal lattices with nominal circular opening diameters of $d_0 = 50–140$ nm and pitches of $p = 0.25–2\ \mu$m. The growth of non-VLS GaAs NWs uses the following procedure: first, a high-temperature substrate annealing step under high As beam equivalent pressure (BEP) of 5.5×10^{-5} mbar was applied to stabilize a Si(111):As 1×1 surface phase needed for producing high-yield SAE growth,[23] followed by the growth of GaAs NWs at growth temperature of 640 °C. The growth of non-catalytic GaAs(Sb,Si) NWs was induced by simultaneously opening the Ga, Sb, and Si shutters depending on the sample. In total, three different NW sample sets were grown either with Si or Sb only, as well as with simultaneous Si and Sb, referred to as GaAs:Si NWs, GaAs(Sb) NWs, and GaAs(Sb):Si NWs, respectively. Undoped GaAs NWs were also grown for comparison, but due to generally poor growth yield (<20%) and aspect ratios similar to those of GaAs:Si NWs, these NWs are primarily discussed in the supplementary material. Unless otherwise noted, all samples were grown for 150 min using Ga flux of 0.35 Å/s, As-BEP and Sb-BEP of 5.5×10^{-5} mbar and 3×10^{-7} mbar ($FF_{Sb} = 0.5\%$), respectively, and a Si dopant flux of $\sim 1.6 \times 10^{12} cm^{-2} s^{-1}$ which corresponds to an equivalent doping concentration of $\sim 1 \times 10^{19}\ cm^{-3}$ in planar GaAs layers.[23] After the growth was terminated, the substrate was cooled down to ambient temperatures with all shutters closed. For optical studies, identical sample sets were prepared but with additional coaxial 5-nm-thick $Al_{0.3}Ga_{0.7}As$ surface passivation layer, followed by a 3-nm-thick GaAs cap to prevent non-radiative surface recombination of the NWs.

The morphology of the as-grown NW arrays was analyzed using scanning electron microscopy (SEM), and exemplary images of the three different samples taken at 45° are shown in Figs. 1(a)–1(c) at 0.25 μm pitch and nominal SiO_2 opening diameter of 50 nm. The NW morphologies show striking differences: GaAs:Si NWs show typical morphologies as reported previously[23] with close to ~100% yield and having a length of $\sim 1000 \pm 200$ nm. GaAs(Sb) NWs show high non-uniformity (despite good yield of ~90%), but there are visibly NWs with very high axial length and also short NWs giving an average length of $\sim 3000 \pm 1200$ nm. Further adding Si dopants significantly improves uniformity in GaAs(Sb):Si NWs, while maintaining lengths that are much longer compared to GaAs:Si NWs grown without Sb.

Quantitative analysis of NW length and diameter (and respective growth rates) was performed for different SiO_2 mask opening diameters for the three characteristic NW samples, in order to better observe the dynamics in morphology evolution. As shown in Figs. 2(a) and 2(b), all samples indicate an inverse length vs diameter dependence that is characteristic of group-III diffusion limited growth in non-VLS NWs.[31,32] Specifically, NWs grown from large mask openings exhibit short NW length at increased NW diameter (poor aspect ratio), while the NW length (diameter) increases (decreases) substantially toward small mask openings. This behavior is more pronounced in GaAs NWs with added Sb, but represents overall the universal nature of non-catalytic growth as also found by other growth methods[31] and in

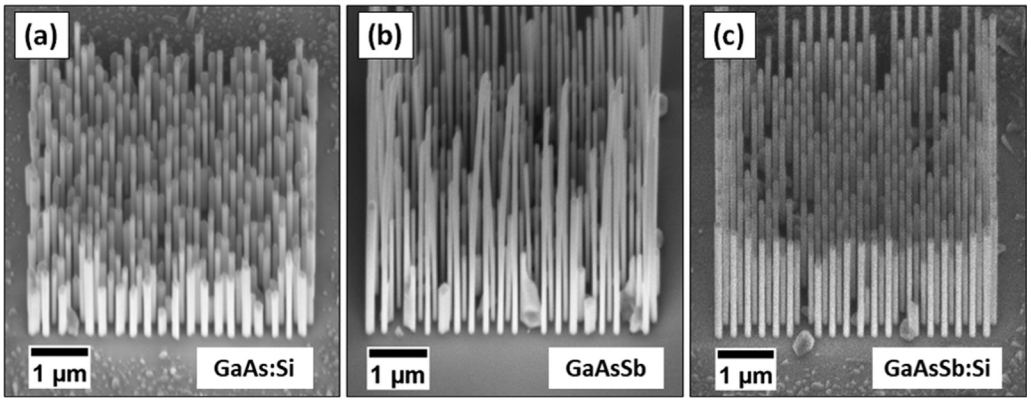

FIG. 1. SEM images of three exemplary NW arrays with pitch 0.25 μm and SiO_2 opening diameter of 50 nm imaged at 45°: (a) GaAs:Si NWs, (b) GaAs(Sb) NWs, and (c) GaAs(Sb):Si NWs (SEM images are tilt corrected to display real lengths).

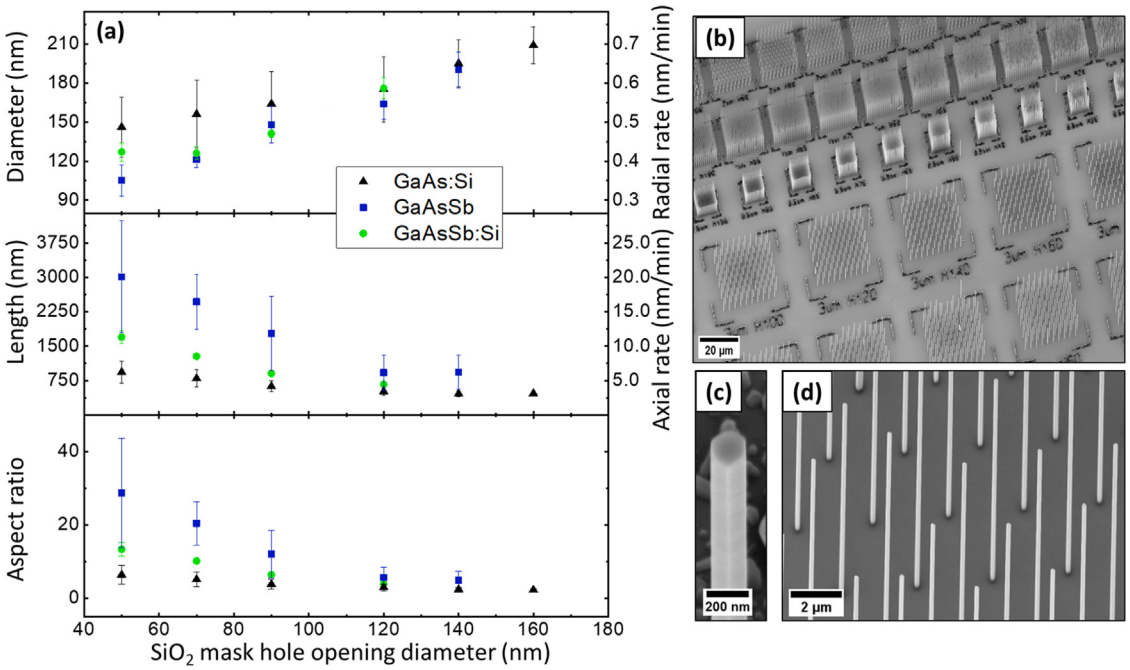

FIG. 2. (a) Quantitative analysis of the average NW diameter, length (and corresponding averaged growth rates), as well as aspect ratio as a function of SiO_2 mask opening size obtained from a statistical analysis of >20 NWs/array for the three respective NW samples grown for 150 min; (b) overview of several fields of GaAs(Sb):Si NW arrays grown under higher Ga-flux (0.7 Å/s); (c) and (d) exemplary close-up views of the taper-free NW morphology and specular (111)B growth facet at the top, shown for an array with pitch of 2 μm and mask opening diameter of 50 nm. (SEM images b, c, and d are tilt corrected to display real lengths).

other materials systems, e.g., InAs and InAsSb NWs.[33] In contrast, self-catalyzed VLS GaAs NWs show a complete independence of NW length and diameter with respect to mask opening size.[34]

Most strikingly, the addition of Sb leads to strongly enhanced axial growth in the limit of small mask opening size. This is evidenced both by the increased aspect ratio and respective axial growth rate, which is also plotted in Fig. 2(b) for generality to give an overall impression. Representation in growth rate units (as often reported in literature) needs to be viewed with care though, since this only provides insight into averaged data (i.e., growth rate = NW length/total growth time) and is strictly valid only under steady-state growth. Based on specific growth time series, we show in the supplementary material that the axial growth dynamics of the present NWs are, however, highly nonlinear with continually increasing axial rates over time. Hence, the actual growth rate at any given time unit cannot be determined, and it is more reasonable to rather discuss axial vs radial growth in absolute terms, by referring in the following to aspect ratio that resulted after a given growth time. For example, for a mask opening of 50 nm the aspect ratio (A.R.) experiences a >4-fold increase from GaAs:Si NWs (A.R. ~7) to GaAs(Sb) NWs (A.R. ~30), when comparing our 150-min growths. Note, undoped GaAs NWs exhibit very similar aspect ratio as GaAs:Si NWs (see the supplementary material), and thus, the strong growth enhancement clearly stems from the effects mediated by Sb. The addition of Si dopants slightly reduces axial growth (A.R. ~15 at d_0 = 50 nm) in GaAs(Sb):Si NWs, but still gives a ~2-fold enhancement over GaAs:Si NWs without Sb. Since in non-VLS growth the axial growth rate is governed by the group-III flux,[24] even further enhancements are expected by increasing the Ga flux rate. This is demonstrated in Figs. 2(b)–2(d), showing high-uniformity arrays of GaAs(Sb):Si NWs grown under twice as large Ga-flux (=0.7 Å/s). These images clearly highlight the advanced scalability of the non-catalytic growth process across a wide array of pattern geometries, and the remarkable uniformity in terms of morphology (taper-free NWs with flat, specular, end facets) and with negligible wire to wire variation. Figure 2(d) illustrates a NW length of ~9 μm at diameter of ~180 nm from a field with small opening diameter (d_0 = 50 nm), leading to very high aspect ratio of ~50.

Overall, our results show two prominent characteristics: first, the addition of Sb strongly enhancing NW growth, and second, co-deposition of Si dopants enhancing uniformity, at the slight expense of aspect ratio. The growth enhancing effect by Sb—that obviously acts as strong self-surfactant—is in surprising contrast to the commonly believed notion that Sb suppresses axial growth while promoting radial growth (i.e., an effect that is aggravated for increased Sb supply). Multiple works reported that the addition of Sb in VLS-GaAs NWs,[29,30] VLS-InAs NW, or VS-InAs NW[33,35–37] strongly suppresses growth, leading to very low aspect ratio NWs, irrespective of the growth method and growth mode. We, therefore, suggest that our unique findings are a specific result at the limit of ultra-low Sb fluxes, where only traces of Sb are present during growth. Using energy-dispersive x-ray (EDX) spectroscopy on both undoped GaAs(Sb) and Si-doped GaAs(Sb):Si NWs confirmed the small traces of Sb (~1.2%–1.9%), which are uniformly distributed along the NW (supplementary material). To understand the mechanism of the strong Sb self-surfactant effect, we suggest enhanced surface diffusion on the NW sidewalls taking place under such trace amounts of Sb. Si

co-dopants, on the other hand, rather act as anti-surfactant, since they reduce aspect ratio and increase radial growth. Deriving a complete understanding of the atomistic origins for the altered growth dynamics requires, however, modeling of surface diffusion energetics and analysis of the modified surface phases of the NW sidewalls, and clearly motivates for future work.

To microscopically study the effects of Sb and Si co-dopants, NWs were transferred from identical fields to carbon-coated copper grids and analyzed by transmission electron microscopy (TEM), electron diffraction, and high-angle annular dark-field scanning transmission electron microscopy (HAADF-STEM) in a FEI Titan Themis operating at 300 kV. TEM micrographs of GaAs:Si NWs, as shown in Fig. 3(a), confirm typical expectations[23,24] as also seen in undoped non-VLS GaAs NWs (supplementary material): They exhibit heavily defected microstructure and a growth front characterized by a pyramidal-shaped tip that is terminated by {110}-type planes. Specifically, these NWs show a very high density of ultrashort ZB-rotational twin domains and stacking defects containing hexagonal stacking, and even a tendency for random layer stacking.[23,24] The majority of NWs further exhibit additional planar defects that are inclined by 20° with respect to the [111]B NW growth axis, which terminate at the NW sidewall. The inclination angle of these faults corresponds to the (−1–11) plane[29] and are also readily observed in undoped non-VLS GaAs NWs (supplementary material). We believe that the combination of these planar faults and the formation of a non-planar, pyramidal top facet might be limiting factors for the growth of GaAs NWs in the absence of surfactants.

In contrast, the addition of Sb results in distinctly different microstructure and growth facet structure. As seen in Figs. 3(b) and 3(c), the growth front clearly evolves as a dominant and flat (111)B-terminated facet, with only minor (−1–10)-like facets in the top corner.[38] Both GaAs(Sb) and GaAs(Sb):Si NWs exhibit a distinct ZB-phase with rotational twin domains only, but no further hexagonal inclusions, as recognized from the high-resolution (HR) HAADF-SEM [Figs. 3(d) and 3(e)] and selected area diffraction (SAD) pattern data. This mimics the typical trend observed also in Au- or Ga-catalyzed VLS-type GaAs(Sb) NWs,[29,30,39,40] where Sb addition stabilizes the ZB-phase. However, as seen from

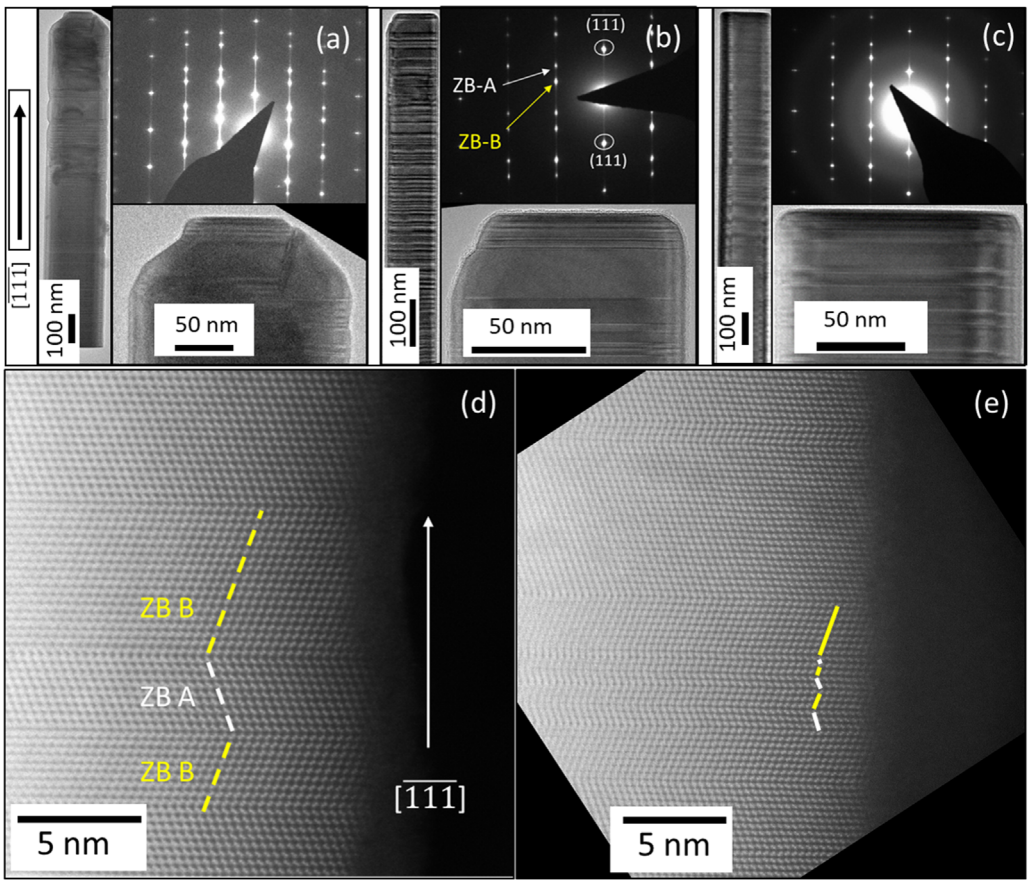

FIG. 3. TEM micrographs and corresponding SAD patterns of representative GaAs:Si NWs (a), GaAs(Sb) NWs (b), and GaAs(Sb):Si NWs (c). Micrographs in the left panel show the general structure and morphology of the NWs, while the micrographs in the bottom panel show the distinctly different facet structure of the NW growth front. The SAD patterns show the growth direction via the diffraction spots indexed as (111) and marked by the white circle; characteristic ZB-A and ZB-B rotational domains are further evident and indexed accordingly for the GaAs(Sb) and GaAs(Sb):Si NWs. HR-HAADF-STEM micrographs illustrate the typical morphology and crystal layer stacking of representative GaAs(Sb) NWs (d) and GaAs(Sb):Si NWs (e). Rotational twin domains are marked in yellow and white.

the HAADF-STEM images of Figs. 3(d) and 3(e), GaAs(Sb):Si displays higher twin densities with several twin domains as short as a single monolayer. Statistical analysis revealed an average twin defect density of ∼0.15 twins/ML for GaAs(Sb):Si NWs and ∼0.05 twins/ML (factor 3 lower) for undoped GaAs(Sb) NWs, respectively. We attribute the quite different twin densities to the effect of Si dopants, since similar trends were also observed from systematic Si-doping studies of Sb-free GaAs NWs (as will be reported elsewhere), while the measured Sb-traces in both NWs are nearly the same (supplementary material).

Twin defects also play an essential role in the growth dynamics of non-catalytic GaAs NWs,[32,38] often referred to as twin-induced growth mode that governs growth rate. Recent studies of undoped GaAs NWs grown by MOVPE showed that the twin-defect density is substantially increased in smaller diameter NWs, enhancing axial NW growth.[38] Our data show rather the opposite trend, with the thinnest NWs [i.e., GaAs(Sb) NWs] exhibiting lowest twin-defect densities, yet fastest axial growth. This affirms that the Sb self-surfactant effect plays the dominating role in the control of growth dynamics of the non-catalytic GaAs NWs presented here.

Finally, the luminescence properties of single NWs were studied by dispersing as-grown NWs to Si substrates and performing excitation power dependent and time-resolved confocal μPL measurements. Hereby, individual NWs, placed in a He-flow cryostat (10 K), were excited using a continuous-wave tunable Ti:Sapphire laser (780 nm) with an excitation spot size of ∼2 μm focused by an objective lens with NA = 0.42. Time-resolved measurements were enabled via time correlated single-photon counting (TCSPC) using a single-photon Si avalanche diode (SPAD) with a time resolution of <365 ps and a PicoHarp 300 module. No spectral filtering was applied, such that the time-resolved data were obtained over the entire emission spectrum. In the following, we compare data from undoped GaAs and GaAs(Sb) NWs, since they allow unambiguous correlation with the underlying structural properties. Luminescence from Si-doped GaAs NWs, on the other hand, is strongly obscured by broad, far-below bandgap luminescence arising from Si dopant-point defect complexes, as reported previously,[23] and therefore not shown here.

Figure 4(a) shows exemplary excitation power dependent μPL spectra with Gaussian fits from a GaAs(Sb) NW (left) and a GaAs NW (right). The PL spectrum from the GaAs NW exhibits typical signatures of polytypic microstructure, characterized by multi-peak emission under low excitation power density.[19,35,44] Here, in fact two distinct peaks are observed, a low-energy peak centered around 1.493 eV and another peak at 1.508 eV (see also inset). With increasing excitation power density, the low-energy peak saturates due to state filling, while the peak at 1.508 eV becomes dominant and rises linearly with excitation power. This behavior reflects the presence of two different excitonic states: a bound state at 1.493 eV that is commonly attributed to spatially indirect excitons arising from the type-II band alignment with the hexagonal inclusions,[19,34,41] and a much weaker bound state or quasi-continuum at 1.508 eV of the otherwise predominant twinned ZB-domain structure.

In contrast, the GaAs(Sb) NWs exhibit single-peak emission throughout the excitation power density range, even at the lowest power density (P = 3.23 μW μm^{-2}). The PL peak is centered near 1.42 eV, i.e., red-shifted by ∼80 meV from the Sb-free GaAs NWs. This is expected from a combination of two effects: the few-percent Sb incorporation in the NW, and the different nature of exciton confinement given the altered microstructure. Particularly, in GaAs(Sb) NWs only twinned ZB domains are present with segment length much longer compared to GaAs NWs. This leads to recombination of quasi-free electrons (reduced quantum confinement) in ZB domains with holes confined at fixed energy level in adjacent rotational twin defects.[41,42] This gives dominant emission at ∼30 meV below the band edge of the pure twin-free crystal and further explains the overall observation of single peak emission.

Time-resolved PL data taken at low excitation power density provide further proof of the structure-dependent differences in exciton

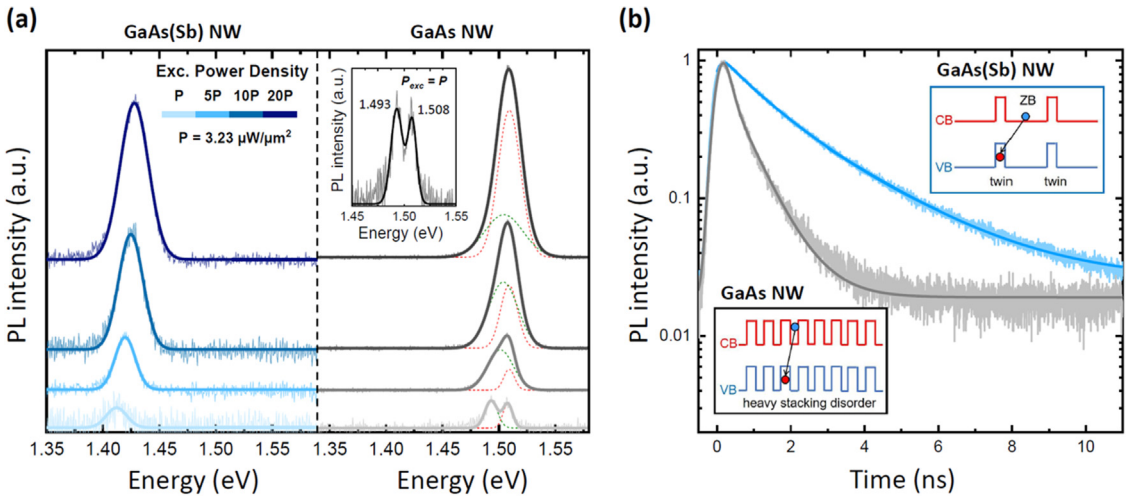

FIG. 4. (a) Micro-PL spectra with Gaussian fits from a single GaAs(Sb) (left)- and GaAs (right) NW recorded at low-temperature (10 K) for different excitation power densities. Spectra are offset for clarity. Inset shows the magnified view of the PL emitted from the GaAs NW, with two distinct peaks at low excitation power density. (b) Time-resolved PL of the two respective NWs recorded at low excitation power density of 100 μW, along with best fits to the data assuming bi-exponential decay characteristics. Insets show schematics of the emission processes of the two different NWs.

localization and recombination dynamics, as shown in Fig. 4(b). Qualitatively, the time decay characteristics of both the GaAs and GaAs(Sb) NWs are described by stretched exponential behavior—due to the presence of bound and quasi-continuum excitonic states—but, notably, the observed decay transients are quantitatively very different. Such stretched exponential decay is commonly approximated by a bi-exponential decay,[43,44] in order to obtain information about the lifetimes of structure-related localized excitons which are essentially captured in the slow decay component of the exponential tail.[44] By fitting the exponential decay transients, which were convoluted with the instrument response function of the experimental setup, we extracted decay times of ∼0.6 ns (fast initial decay) and ∼1 ns (slow decay component) for Sb-free non-VLS GaAs NWs. The initial faster decay time is attributed to the quasi-continuum states, while the slow decay time represents the long-lived type-II indirect exciton transitions arising from the intermixed layer stacking. Importantly, the slow decay time gets much longer (∼4 ns) for the GaAs(Sb) NWs. Such remarkably increased exciton lifetime is characteristic for enhanced spatial separation of electron-hole pairs at type-II twin domain heterostructures,[44] reflecting the changes in the crystal structure compared to the Sb-free GaAs NWs. We also performed measurements under increased excitation power density (not shown), revealing expected shorter lifetimes (down to ∼2 ns) due to increased spatial overlap of e-h pairs and eventually carrier escape at the twin boundaries. This situation is best illustrated by the schematic emission processes depicted in the insets of Fig. 4(b) for the limit of low carrier excitation. Heavy stacking disorder with short-period alterations of cubic and hexagonal stacking (case of GaAs NWs) causes strong quantum confinement of both electrons and holes, and hence, less spatial separation of e–h pairs. In contrast, ZB domain structure with extended ZB segments separated by rotational twin defects [case of GaAs(Sb) NWs] induce extended electron wavefunction distribution, i.e., quasi-free electrons in the ZB domains, allowing for larger separation of e–h pairs.[41,42] Hence, our studies clearly demonstrate how the addition of small traces of Sb modifies not only the underlying microstructure but also the principles of carrier and exciton dynamics in these new generations of non-VLS-based GaAs NWs.

See the supplementary material for SEM images of undoped and Si-doped GaAs NWs comparing yield and morphology, yield of undoped and Si-doped GaAs(Sb) NWs, EDX analysis of undoped and Si-doped GaAs(Sb) NWs, additional TEM data of undoped GaAs NWs, dynamic growth rates, and possible role of Sb in enhancing diffusion.

This work was supported by the European Research Council (ERC project QUANtIC, ID: 771747) and the Deutsche Forschungsgemeinschaft (DFG) via Germany's Excellence Strategy-EXC-2111-390814868 (Munich Center for Quantum Science and Technology, MCQST). The authors also thank H. Riedl for technical support with MBE, and Paul Schmiedeke and Fabio del Giudice for fruitful discussions.

AUTHOR DECLARATIONS

Conflict of Interest

The authors have no conflicts to disclose.

Author Contributions

Akhil Ajay: Conceptualization (equal); Data curation (equal); Formal analysis (equal); Investigation (equal); Methodology (equal); Validation (equal); Visualization (equal); Writing – original draft (equal); Writing – review and editing (equal). **Hyowon Jeong:** Data curation (equal); Investigation (equal); Visualization (equal). **Tobias Schreitmüller:** Data curation (equal); Formal analysis (equal). **Markus Döblinger:** Data curation (equal); Formal analysis (equal). **Daniel Ruhstorfer:** Data curation (equal); Formal analysis (equal). **Nitin Mukhundhan:** Data curation (equal); Formal analysis (equal). **Philemon Koolen:** Data curation (equal); Formal analysis (equal). **Jonathan J. Finley:** Conceptualization (equal); Supervision (equal). **Gregor Koblmüller:** Conceptualization (equal); Formal analysis (equal); Funding acquisition (equal); Investigation (equal); Project administration (equal); Resources (equal); Supervision (equal); Validation (equal); Writing – original draft (equal); Writing – review and editing (equal).

DATA AVAILABILITY

The data that support the findings of this study are available within the article and its supplementary material. Additional supporting data can be obtained from the authors.

REFERENCES

[1]D. Saxena, S. Mokkapati, P. Parkinson, N. Jiang, Q. Gao, H. H. Tan, and C. Jagadish, Nat. Photon. **7**, 963 (2013).
[2]J. Tatebayashi, S. Kako, J. Ho, Y. Ota, S. Iwamoto, and Y. Arakawa, Nat. Photon. **9**, 501 (2015).
[3]B. Mayer, L. Janker, B. Loitsch, J. Treu, T. Kostenbader, S. Lichtmannecker, T. Reichert, S. Morkötter, M. Kaniber, G. Abstreiter, C. Gies, G. Koblmüller, and J. J. Finley, Nano Lett. **16**, 152 (2016).
[4]B. Loitsch, J. Winnerl, G. Grimaldi, J. Wierzbowski, D. Rudolph, S. Morkötter, M. Döblinger, G. Abstreiter, G. Koblmüller, and J. J. Finley, Nano Lett. **15**, 7544 (2015).
[5]L. Leandro, C. P. Gunnarsson, R. Reznik, K. D. Jöns, I. Shtrom, A. Khrebtov, T. Kasama, V. Zwiller, G. Cirlin, and N. Akopian, Nano Lett. **18**, 7217 (2018).
[6]N. Mukhundhan, A. Ajay, J. Bissinger, J. J. Finley, and G. Koblmüller, Opt. Express **29**, 43068 (2021).
[7]P. Krogstrup, H. I. Jørgensen, M. Heiss, O. Demichel, J. V. Holm, M. Aagesen, J. Nygard, and A. Fontcuberta i Morral, Nat. Photon. **7**, 306 (2013).
[8]I. Åberg, G. Vescovi, D. Asoli, U. Naseem, J. P. Gilboy, C. Sundvall, A. Dahlgren, K. E. Svensson, N. Anttu, M. T. Bjork, and L. Samuelson, IEEE J. Photovolt. **6**, 185 (2016).
[9]A. C. Farrell, X. Meng, D. Ren, H. Kim, P. Senanayake, N. Y. Hsieh, Z. Rong, T. Chang, K. M. Azizur-Rahman, and D. L. Huffaker, Nano Lett. **19**, 582 (2019).
[10]K. Tomioka, M. Yoshimura, and T. Fukui, Nat. **488**, 189 (2012).
[11]J. Wong-Leung, I. Yang, Z. Li, S. K. Karuturi, L. Fu, H. H. Tan, and C. Jagadish, Adv. Mater. **32**, 1904359 (2020). and references therein.
[12]G. Priante, F. Glas, G. Patriarche, K. Pantzas, F. Oehler, and J. Harmand, Nano Lett. **16**, 1917 (2016).
[13]V. G. Dubrovskii, J. Phys. D: Appl. Phys. **50**, 453001 (2017).
[14]A. Darbandi, J. C. McNeil, A. Akhtari-Zavareh, S. P. Watkins, and K. L. Kavanagh, Nano Lett. **16**, 3982 (2016).
[15]F. Panciera, Z. Baraissov, G. Patriarche, V. G. Dubrovskii, F. Glas, L. Travers, U. Mirsaidov, and J. Harmand, Nano Lett. **20**, 1669 (2020).
[16]T. Rieger, S. Heiderich, S. Lenk, M. I. Lepsa, and D. Grützmacher, J. Cryst. Growth **353**, 39 (2012).
[17]J. Tersoff, Nano Lett. **15**, 6609 (2015).
[18]P. Schroth, M. Köhl, J. Hornung, E. Dimakis, C. Somaschini, L. Geelhaar, A. Biermanns, S. Bauer, S. Lazarev, U. Pietsch, and T. Baumbachet, al., Phys. Rev. Lett. **114**, 055504 (2015).

[19]D. Spirkoska, J. Arbiol, A. Gustafsson, S. Conesa-Boj, F. Glas, I. Zardo, M. Heigoldt, M. H. Gass, A. L. Bleloch, S. Estrade, M. Kaniber, J. Rossler, F. Peiro, J. R. Morante, G. Abstreiter, L. Samuelson, and A. Fontcuberta i Morral, Phys. Rev. B **80**, 245325 (2009).
[20]M. M. Sonner, D. Rudolph, G. Koblmüller, and H. J. Krenner, Phys. Rev. Appl. **16**, 034010 (2021).
[21]K. Tomioka, J. Motohisa, S. Hara, K. Hiruma, and T. Fukui, Nano Lett. **10**, 1639 (2010).
[22]J. Noborisaka, J. Motohisa, and T. Fukui, Appl. Phys. Lett. **86**, 213102 (2005).
[23]D. Ruhstorfer, S. Mejia, M. Ramsteiner, M. Döblinger, H. Riedl, J. J. Finley, and G. Koblmüller, Appl. Phys. Lett. **116**, 052101 (2020).
[24]D. Rudolph, S. Hertenberger, S. Bolte, W. Paosangthong, D. Spirkoska, M. Döblinger, M. Bichler, J. J. Finley, G. Abstreiter, and G. Koblmüller, Nano Lett. **11**, 3848 (2011).
[25]B. Ketterer, E. Mikheev, E. Uccelli, and A. Fontcuberta i Morral, Appl. Phys. Lett. **97**, 223103 (2010).
[26]H. Hijazi, G. Monier, E. Gil, A. Trassoudaine, C. Bougerol, C. Leroux, D. Castellucci, C. Robert-Goumet, P. E. Hoggan, Y. André, N. I. Goktas, R. R. LaPierre, and V. G. Dubrovskii, Nano Lett. **19**, 4498 (2019).
[27]J. C. Harmand, L. H. Li, G. Patriarche, and L. Travers, Appl. Phys. Lett. **84**, 3981 (2004).
[28]R. R. Wixom, L. W. Rieth, and G. B. Stringfellow, J. Cryst. Growth **265**, 367 (2004).
[29]X. Yuan, P. Caroff, J. Wong-Leung, H. H. Tan, and C. Jagadish, Nanoscale **7**, 4995 (2015).
[30]D. Ren, D. L. Dheeraj, C. Jin, J. S. Nilsen, J. Huh, J. F. Reinertsen, A. M. Munshi, A. Gustafsson, A. T. J. van Helvoort, H. Weman, and B. O. Fimland, Nano Lett. **16**, 1201 (2016).
[31]K. Ikejiri, T. Sato, H. Yoshida, K. Hiruma, J. Motohisa, S. Hara, and T. Fukui, Nanotechnol. **19**, 265604 (2008).
[32]G. Koblmüller, S. Hertenberger, K. Vizbaras, M. Bichler, F. Bao, J. Zhang, and G. Abstreiter, Nanotechnol. **21**, 365602 (2010).
[33]D. Ruhstorfer, A. Lang, S. Matich, M. Döblinger, H. Riedl, J. J. Finley, and G. Koblmüller, Nanotechnol. **32**, 135604 (2021).
[34]D. Rudolph, L. Schweickert, S. Morkötter, B. Loitsch, S. Hertenberger, J. Becker, M. Bichler, G. Abstreiter, J. J. Finley, and G. Koblmüller, Appl. Phys. Lett. **105**, 033111 (2014).
[35]M. J. L. Sourribes, I. Isakov, M. Panfilova, H. Liu, and P. A. Warburton, Nano Lett. **14**, 1643 (2014).
[36]E. A. Anyebe, M. K. Rajpalke, T. D. Veal, C. J. Jin, Z. M. Wang, and Q. D. Zhuang, Nano Res. **8**, 1309 (2015).
[37]H. Potts, M. Friedl, F. Amaduzzi, K. Tang, G. Tütüncüoglu, F. Matteini, E. Alarcon Lladó, P. C. McIntyre, and A. Fontcuberta i Morral, Nano Lett. **16**, 637 (2016).
[38]H. Yoshida, K. Ikejiri, T. Sato, S. Hara, E. Hiruma, J. Motohisa, and T. Fukui, J. Cryst. Growth **312**, 52 (2009).
[39]D. L. Dheeraj, G. Patriarche, L. Largeau, H. L. Zhou, A. T. J. Van Helvoort, F. Glas, J. C. Harmand, B. O. Fimland, and H. Weman, Nanotechnol. **19**, 27505 (2008).
[40]L. Li, D. Pan, Y. Xue, X. Wang, M. Lin, D. Su, Q. Zhang, X. Yu, H. So, D. Wei, B. Sun, P. Tan, A. Pan, and J. Zhao, Nano Lett. **17**, 622 (2017).
[41]M. M. Sonner, M. Gnedel, J. C. Berlin, D. Rudolph, G. Koblmüller, and H. J. Krenner, Nanotechnol. **32**, 505209 (2021).
[42]A. Senichev, P. Corfdir, O. Brandt, M. Ramsteiner, S. Breuer, J. Schilling, L. Geelhaar, and P. Werner, Nano Res. **11**, 4708 (2018).
[43]C. C. Chang, C. Y. Chi, M. Yao, N. Huang, C. C. Chen, J. Theiss, A. W. Bushmaker, S. LaLumondiere, T. W. Yeh, M. L. Povinelli, C. Zhou, P. D. Dapkus, and S. B. Cronin, Nano Lett. **12**, 4484 (2012).
[44]D. Rudolph, L. Schweickert, S. Morkötter, L. Hanschke, S. Hertenberger, M. Bichler, G. Koblmüller, G. Abstreiter, and J. J. Finley, New J. Phys. **15**, 113032 (2013).